Two-Phase Prototype Filter Design for FBMC Systems

Jiangang Wen[1], Jingyu Hua[1(✉)], Zhijiang Xu[1], Weidang Lu[1], and Jiamin Li[2]

[1] College of Information Engineering, Zhejiang University of Technology, Hangzhou 310023, China
eehjy@163.com
[2] National Mobile Communications Research Laboratory, Southeast University, Nanjing 210096, China

Abstract. FBMC has been taken as a candidate waveform for the next enhanced 5th generation (5G). To further improve its advantages over OFDM as well as to promote its application in burst transmission, a two-phase method is applied to design its prototype filter, i.e. a square-root Nyquist filter. In this method, the autocorrelation-based technique and a spectral factorization aimed at minimum stopband energy are successively exploited to acquire the final prototype filter. Through the relaxation of Nyquist condition and benefited from the nonlinear-phase, the frequency selectivity of our designed filters can be greatly improved. Furthermore, the performances of the proposed prototype filter brings a better BER in simulations, which demonstrates the effectiveness of our square-root Nyquist filter design for FBMC systems.

Keywords: FBMC · Prototype filter · Square-root Nyquist
Spectral factorization

1 Introduction

The evolution toward 5G includes an enhancement of the current cellular network, because the celebrated OFDM suffers from inefficiency for its tight synchronization and the use of cyclic prefix (CP) [1]. Besides, its large out-of-band (OOB) radiation makes it unattractive for flexible access to fragmented spectrum, which is crucial for efficient opportunistic communications in Internet of Things (IoT) [2].

To tackle above issues, a filter bank based multicarrier (FBMC) modulation is proposed as a promising candidate. Although FBMC was first investigated in the 1960s [3], it is experiencing renewed interest and has gained high attention in the recent years. In contrast to OFDM, this non-orthogonal waveform employs high quality filters on every subcarrier to produce better time-frequency localization and very low OOB radiation, and the offset quadrature amplitude modulation (OQAM) is usually employed to further reduce the inter-carrier interference [4]. Moreover, in the application of cognitive radios (CR), FBMC can simultaneously be used for data transmission as well as spectrum sensing [5]. However, the subcarrier-based shaping results in a prototype filter with long impulse response [6].

X. Gu et al. (Eds.): MLICOM 2017, Part II, LNICST 227, pp. 96–105, 2018.
https://doi.org/10.1007/978-3-319-73447-7_12

The prototype filter for subcarrier shaping definitely determined the characteristics of the FBMC, and the nearly perfect reconstruction (NPR) is preferred in the design of prototype filter in discrete-time, such as the square-root raised-cosine (SRRC) filters [7]. There had been two typical design methods in [8, 9]. The frequency sampling technique was applied in the first method, and the obtained prototype filters had exact stopband zeros at the frequencies that were integer multiples of the sub-channel spacing. Nevertheless, the poor tradeoff between Nyquist condition and stopband performance made it inflexible. By contrast, in the second method, the filter could be designed through the minimization of a cost function that suitably struck a balance between stopband attenuation and residual inter-symbol interference (ISI).

Similar to above second method, we will design the square-root (SR) Nyquist filter as prototype filters in FBMC systems, where we straightly do tradeoff between stopband attenuation and residual ISI by constraining both the Nyquist condition and the stopband energy. Moreover, to address the nonconvex problem due to the convolution in transceivers, the autocorrelation-based technique [10] is employed in the construction of linear programming model, leading to linear inequations for ISI control. Besides, the original object and constraints in the stopband must be transformed to the ones about autocorrelation coefficients, i.e., the impulse coefficients of a Nyquist filter. Subsequently, to retrieve the SR Nyquist filter, from the optimized autocorrelation coefficients, a spectral factorization should be applied. Different from conventional minimum phase factorization [11] or the best stopband attenuation factorization [12], the minimum stopband energy is proposed here as the criteria. Such factorization would almost maintain the performances acquired in previous linear programming, and the obtained SR Nyquist filter is a nonlinear-phase one. Compared with the widely-used PHYDYAS filter [4], this resulted nonlinear-phase feature can benefit both the stopband attenuation and group-delay, or reduce the filter length. Thereby, the problems in realization complexity as well as low latency transmission might be alleviated. In our computer simulations, both the filter performances and the BER tests demonstrate a superiority of our designed prototype filters over the PHYDYAS filter.

2 Preliminaries

In the OQAM-FBMC system, the length of a prototype filter satisfies $N_p = KM + 1$, where M and K denote the subcarrier number and the overlapping factor. Thus, a FIR prototype filter can be presented by the real-valued impulse response coefficients $h(n)$, $0 \le n \le N_p - 1$, or its frequency response

$$H(\omega, \mathbf{h}) = \sum_{n=0}^{N_p-1} h(n) e^{-j\omega n} \tag{1}$$

where $\mathbf{h} = [h(0), h(1), \cdots, h(N_p - 1)]$. The frequency response (1) is a general expression for either linear-phase or nonlinear-phase filter.

To design a NPR filter for the FBMC system, both the frequency selectivity and Nyquist condition should be taken into account. For the first purpose, the basic optimization model could be established as

$$\min_{\mathbf{h}} f(\mathbf{h}) \quad s.t. \begin{cases} |H(\omega,\mathbf{h})| \le 1+\delta_p^m, & \omega \in [0,\omega_p] \\ -|H(\omega,\mathbf{h})| \le -1+\delta_p^m, & \omega \in [0,\omega_p] \\ |H(\omega,\mathbf{h})| \le \delta_s^m, & \omega \in [\omega_s,\pi] \end{cases} \tag{2}$$

where the amplitude ripples in both passband and stopband are constrained, and the choice of object function $f(\mathbf{h})$ could be the minimax cost or the least-square cost. In previous design [12], the minimax cost, i.e., the stopband attenuation is chosen, while our study chooses the least-square cost (the stopband energy) as the cost for improved OOB radiation reduction. To solve such an optimization problem (2), a number of algorithms [10, 11] could be exploited.

In practice, the interferences caused by relaxed Nyquist condition are small enough compared to the residual interferences due to transmission channel [13]. Therefore, a constraint for the control of Nyquist condition should be added into the basic model (2), but difficulty appears because of the convolution relation between the Nyquist filter $g(n)$ and its square-root Nyquist filter $h(n)$, i.e. $h(n) \otimes h(-n)$. This convolution makes the time-domain Nyquist constraints are nonconvex about $h(n)$

$$\sum_{kM \neq (N-1)/2} |g(kM)|^2 \le \phi_t \tag{3}$$

where ϕ_t represents the pre-specified threshold for relaxed Nyquist condition and $N = 2N_p - 1$ denotes the filter length of $g(n)$. In above constraints, M is an integer usually called the over-sampling factor, and it is exactly equal to the number of subcarrier number.

In order to solve the above nonconvex issue of $h(n)$, we will design $g(n)$ first and then factorize it into $h(n)$'s, which is analogous to previous study [12]. However, our study employs the least-squares stopband ripples instead of the minimax in [12]. Moreover, the Nyquist condition in our study is established in frequency-domain based on the power-complementary property.

3 The Prototype Filter Design

The proposed method for prototype filter (SR Nyquist filter) design includes two steps. Firstly, the mathematical model is established and the optimization can be conducted with different constraint thresholds. In this step, the controllable inequation for Nyquist condition in the frequency-domain is expressed as a linear one, meanwhile the requirement for frequency selectivity is transformed to constrain the autocorrelation coefficient $g(n)$. In the second step, a spectral factorization is applied to the NYQ filter obtained in the previous step, resulting in the square-root Nyquist filter or the prototype

filter ($h(n)$) equivalently. Note that the factorization also aims at the minimum stopband energy as we have done in the optimization step.

3.1 The NYQ Filter Design and Factorization

For Nyquist condition, we have the property of power complementary in the frequency-domain [9].

$$\sum_{k=0}^{M-1} \left| G(e^{j(\omega+\frac{2\pi}{M}k)}) \right| = 1,\ 0 \le \omega \le \pi/M \tag{4}$$

where $G(e^{j\omega})$ is the frequency response of the Nyquist filter $g(n)$. Due to its linear phase, $G(e^{j\omega})$ can be simplified to its zero-phase response $A(\omega, \mathbf{g})$ by abandoning the linear-phase term $e^{-j\omega(N-1)/2}$, which can be represented by using $\mathbf{g} = [g(0), g(1), \cdots, g((N-1)/2)]^T$, i.e.,

$$A(\omega, \mathbf{g}) = \mathbf{c}^T(\omega)\mathbf{g} \tag{5}$$

with $\mathbf{c}(\omega) = \left[2\cos(\omega\frac{N-1}{2}), 2\cos(\omega\frac{N-3}{2}), \cdots, 2\cos(\omega), 1\right]^T$

According to the Nyquist condition in time-domain, a measurement to evaluate fitler's robustness against ISI was established in [12]. The better the Nyquist condition is satisfied, the smaller will this measurement be. Analogously, based on above power complementary, the measurement in frequency-domain is defined as the formula about $A(\omega, \mathbf{g})$, i.e.,

$$ISI_p = \int_0^{\frac{\pi}{M}} \left| \sum_{k=0}^{M-1} A(\omega + \frac{2\pi}{M}k, \mathbf{g}) - 1 \right|^p, p \ge 1 \tag{6}$$

For convenience, let

$$A_S(\omega, \mathbf{g}) = \sum_{k=0}^{M-1} A(\omega + \frac{2\pi}{M}k, \mathbf{g}) \tag{7}$$

And in our design, let $p \to \infty$, thus the formula (6) turns to

$$ISI = |A_S(\omega, \mathbf{g}) - 1|_{\max}, 0 \le \omega \le \pi/M \tag{8}$$

Then, it allows us to establish the frequency domain constraint by the simple forms

$$\begin{cases} A_S(\omega, \mathbf{g}) - 1 \le \phi_f, & 0 \le \omega \le \pi/M \\ -A_S(\omega, \mathbf{g}) + 1 \le \phi_f, & 0 \le \omega \le \pi/M \end{cases} \tag{9}$$

where ϕ_f is the pre-specified threshold for Nyquist control. As it is relaxed, better frequency selectivity would be traded for even the reduced filter length.

To keep consistency in the variable to be optimized, former model (2) must be transformed. First, the choice of object function should be done by representing it as

$$f(\mathbf{h}) = \int_{\omega_s}^{\pi} |H(\omega, \mathbf{h})|^2 d\omega \tag{10}$$

It means that the energy in stopband will be minimized in the design for prototype filter. The reason for this choice is that it has a similar effect as the minimization of OOB radiation, and the stopband attenuation is gradually promoted as the frequency far from the transition band. Besides, in following spectral factorization, this cost choice could produce a particularity that can reduce the complexity of finding the best SR Nyquist filter. Thanks to the relation between $A(\omega, \mathbf{g})$ and $H(\omega, \mathbf{h})$, i.e., $A(\omega, \mathbf{g}) = |H(\omega, \mathbf{h})|^2$, the object function can be readily transformed to the one aiming at $g(n)$

$$f(\mathbf{g}) = \int_{\omega_s}^{\pi} A(\omega, \mathbf{g}) d\omega = \mathbf{s}^T(\omega)\mathbf{g} \tag{11}$$

with the definition

$$\mathbf{s}(\omega) = \left[-4\frac{\sin(\omega_s \cdot \frac{N-1}{2})}{N-1}, -4\frac{\sin(\omega_s \cdot \frac{N-3}{2})}{N-3}, \cdots, -4\frac{\sin(\omega_s)}{2}, \pi - \omega_s \right]$$

Correspondingly, the constraint inequations for amplitude ripples are also modified, but just like many cases, in our final optimization model, only the stopband part is considered in constraints, and the ripples in passband is inherently shaped. Thus, the inequation for passband ripples is avoided, and the design problem could be expressed as to

$$\begin{aligned} &\min_{\mathbf{g}} f(\mathbf{g}) = \mathbf{s}^T(\omega)\mathbf{g} \\ &s.t. \begin{cases} A_S(\omega, \mathbf{g}) - 1 \le \phi_f, & \omega \in \left[0, \frac{\pi}{M}\right] \\ -A_S(\omega, \mathbf{g}) + 1 \le \phi_f, & \omega \in \left[0, \frac{\pi}{M}\right] \\ \mathbf{c}^T(\omega)\mathbf{g} \le \left(\delta_s^m\right)^2, & \omega \in [\omega_s, \pi] \\ \mathbf{c}^T(\omega)\mathbf{g} \ge 0, & \omega \in [0, \pi) \end{cases} \end{aligned} \tag{12}$$

Among these constraint inequations, the third is the constraint for stopband attenuation, and the last one represents the condition for $g(n)$ to be the corresponding autocorrelation of $h(n)$. Consequently, this optimization problem can be easily solved by linear programming. Note that, though the design problem is with respect to $g(n)$, it is definitely optimized for the prototype filter as long as it could be retrieved by spectral factorization.

After getting the autocorrelation coefficients $g(n)$, the spectral factorization for minimum stopband energy is carried out to retrieve the prototype filter $h(n)$. which is analogous to those in [12]. An example with $M = 8$ and several different values of ϕ_f can be found in Fig. 1. In these figures, the nearly superposed zero pairs on the unit

circle are partitioned into two different zero groups, which determine the frequency response of stopband. Meanwhile, the other reciprocal pairs are uniformly separated, which would limit the passband ripples. The final zero groups '○' and '*' explicitly make up the obtained subfilter subfilters '**h**1' and '**h**2'.

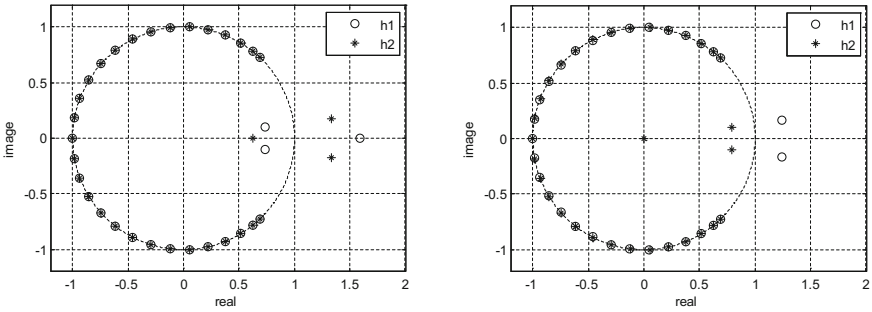

a. $\phi_f = 0.6 \cdot 10^{-3}$ b. $\phi_f = 8.0 \cdot 10^{-3}$

Fig. 1. The spectral factorization results for $M = 8$ and different ϕ_f's.

3.2 Filter Design Examples

First, we define the typical performance indicators include the passband ripples (R_p), the stopband attenuation (A_s), the stopband energy (E_s), the deviation of Nyquist in time-domain (ISI_t) [9] and in frequency-domain (ISI_f), viz.,

$$\begin{cases} R_p = -20\lg(1-\delta_p)\ , \delta_p = \max\limits_{\omega\in[0,\omega_p]} ||F(\omega)| - 1| \\ A_s = -20\lg(\delta_s)\ \ , \delta_s = \max\limits_{\omega\in[\omega_s,\pi]} |F(\omega)| \\ E_s = \mathbf{s}^T(\omega)\mathbf{g}\ \ or\ \ E_s = \int_{\omega_s}^{\pi} |H(\omega,\mathbf{h})|^2 d\omega \\ ISI_t = \sum\limits_{d=1}^{K} \frac{\left|\mathbf{g}\left(\frac{N-1}{2}+dM\right)\right| + \left|\mathbf{g}\left(\frac{N-1}{2}-dM\right)\right|}{\left|\mathbf{g}\left(\frac{N-1}{2}\right)\right|}, ISI_f = \max\limits_{\omega\in[0,\frac{\pi}{M}]} \left| \sum\limits_{k=0}^{M-1} A(\omega+\frac{2\pi}{M}k, \mathbf{g}) - 1 \right| \end{cases} \tag{13}$$

Referring to the FBMC setting in [13], we set $M = 8$ and $K = 4$, which leads to $N_p = 33$ for the prototype filter and $N = 65$ for the Nyquist filter. Due to the OQAM modulation, the roll-off factor is typically chosen as $\alpha = 1.0$, i.e., the same choice of PHYDYAS filter [13], which results in $\{\omega_c = \pi/M, \omega_s = 2\pi/M\}$. Meanwhile, the pre-specified threshold ϕ_f for Nyquist condition are relaxed to some different extent $\{0.6, 1, 4:4:12\} \cdot 10^{-3}$ for better frequency selectivity. The numerical results are listed in Table 1. Note that $F(\omega)$ in above formula should be chosen as $A(\omega, \mathbf{g})$ or $H(\omega, \mathbf{h})$ for $g(n)$ or $h(n)$.

From Table 1, we can clearly see the effectiveness of the Nyquist constraint in frequency-domain, where the resulted ISI_t and ISI_f are nearly the same. Moreover, a larger ϕ_f brings improvements both on A_s and E_s, which is beneficial for FBMC

Table 1. The performances of the Nyquist filter by optimization model (12) ($M = 8$).

ϕ_f	$R_p(dB)$	$A_s(dB)$	E_s	ISI_t	ISI_f
$0.6 \cdot 10^{-3}$	6.0258	105.1592	$1.6808 \cdot 10^{-7}$	$6.10 \cdot 10^{-4}$	$6.00 \cdot 10^{-4}$
$1.0 \cdot 10^{-3}$	6.0293	105.3603	$1.6283 \cdot 10^{-7}$	$1.00 \cdot 10^{-3}$	$1.00 \cdot 10^{-3}$
$4.0 \cdot 10^{-3}$	6.0554	106.9512	$1.2334 \cdot 10^{-7}$	$4.00 \cdot 10^{-3}$	$4.00 \cdot 10^{-3}$
$8.0 \cdot 10^{-3}$	6.0904	109.6685	$7.0680 \cdot 10^{-8}$	$8.00 \cdot 10^{-3}$	$8.00 \cdot 10^{-3}$
$1.20 \cdot 10^{-2}$	6.1255	116.8648	$3.3380 \cdot 10^{-8}$	$1.20 \cdot 10^{-2}$	$1.20 \cdot 10^{-2}$

prototype filter requiring better stopband suppression in FBMC. Such kind of tradeoff is exactly what the PHYDYAS does not achieve. Besides, we also show the spectral factorization results in Table 2, where the obtained A_s and R_p is nearly half of those in Table 1. Additionally, the resulted ISI_t and ISI_f in Table 2 are nearly the same as those before spectral factorization. All of those demonstrate that the two-phase method including constrained optimization and spectral factorization is effective for NPR prototype filter design.

Table 2. The performances of the subfilters after proposed spectral factorization ($M = 8$).

ϕ_f		$0.6 \cdot 10^{-3}$	$1.0 \cdot 10^{-3}$	$4.0 \cdot 10^{-3}$	$8.0 \cdot 10^{-3}$
$R_p(dB)$	**h**1	3.0009	3.0071	3.0313	3.0595
	h2	3.0301	3.0308	3.0588	3.1000
$A_s(dB)$	**h**1	52.2281	52.3485	53.1431	54.4826
	h2	52.9361	53.0204	53.8427	55.2551
E_s	**h**1	$1.6957 \cdot 10^{-7}$	$1.6394 \cdot 10^{-7}$	$1.2434 \cdot 10^{-7}$	$7.2396 \cdot 10^{-8}$
	h2	$1.6717 \cdot 10^{-7}$	$1.6206 \cdot 10^{-7}$	$1.2193 \cdot 10^{-7}$	$6.8386 \cdot 10^{-8}$
ISI_t		$6.10 \cdot 10^{-4}$	$1.00 \cdot 10^{-3}$	$4.00 \cdot 10^{-3}$	$8.00 \cdot 10^{-3}$
ISI_f		$5.94 \cdot 10^{-4}$	$0.99 \cdot 10^{-3}$	$4.00 \cdot 10^{-3}$	$7.90 \cdot 10^{-3}$

4 Simulation and Analysis

In this section, the prototype filter designed by the proposed two-phase method is compared with the PHYDYAS filter promoted by 5GNOW in terms of both the filter performance and the bit-error-ratio (BER).

4.1 The Comparison with the PHYDYAS Filter

In the first comparison of performances, only the retrieved subfilters '**h**1' are adopted with the constraint thresholds $\phi_f = \{0.6, 4, 12\} \cdot 10^{-3}$, since subfilters '**h**2' produces the same performances. The comparison results are presented in Table 3, and for convenience the PHYDYAS is abbreviated to PHY.

Explicitly, the proposed prototype filters outperform the PHYDYAS filter for the same K. Meanwhile, the E_s gaps of two kinds of filters could be up to two orders of

Table 3. The comparison between the prototype filters in our design and the PHY filters.

$M = 8$	N_p	$R_p(dB)$	$A_s(dB)$	E_s	ISI_t	ISI_f
PHY_A, $K = 4$	33	3.0103	39.8582	$1.0759 \cdot 10^{-5}$	$0.82 \cdot 10^{-3}$	$0.63 \cdot 10^{-3}$
PHY_B, $K = 3$	25	2.9946	32.5643	$8.0357 \cdot 10^{-5}$	$4.10 \cdot 10^{-3}$	$3.80 \cdot 10^{-3}$
$\mathbf{h1}_A$, $K = 4$, $\phi_f = 0.6 \cdot 10^{-3}$	33	3.0009	52.2281	$1.6957 \cdot 10^{-7}$	$0.61 \cdot 10^{-3}$	$0.59 \cdot 10^{-3}$
$\mathbf{h1}_B$, $K = 4$, $\phi_f = 4.0 \cdot 10^{-3}$	33	3.0313	53.1431	$1.2434 \cdot 10^{-7}$	$4.00 \cdot 10^{-3}$	$4.00 \cdot 10^{-3}$
$\mathbf{h1}_C$, $K = 4$, $\phi_f = 1.2 \cdot 10^{-2}$	33	3.0947	58.1638	$3.3758 \cdot 10^{-8}$	$1.20 \cdot 10^{-2}$	$1.19 \cdot 10^{-2}$
$\mathbf{h1}_D$, $K = 3$, $\phi_f = 0.6 \cdot 10^{-3}$	25	2.9870	38.8187	$4.6365 \cdot 10^{-6}$	$0.77 \cdot 10^{-3}$	$0.72 \cdot 10^{-3}$
$\mathbf{h1}_E$, $K = 3$, $\phi_f = 4.0 \cdot 10^{-3}$	25	2.9871	38.9423	$4.4688 \cdot 10^{-6}$	$4.20 \cdot 10^{-3}$	$4.10 \cdot 10^{-3}$
$\mathbf{h1}_F$, $K = 3$, $\phi_f = 1.2 \cdot 10^{-2}$	25	2.9874	39.2507	$4.0704 \cdot 10^{-6}$	$1.21 \cdot 10^{-2}$	$1.23 \cdot 10^{-2}$

magnitudes. Due to the nearly equivalent relation between E_s and OOB radiation, the improved E_s must be beneficial in many applications such as CR network. On the other hand, thanks to the flexible tradeoff in our method, it might be possible to reduce the filter length by replacing smaller value of K. In Table 3, it can be seen that the filter performances are sacrificed in our filter of $K = 3$, but it still produces comparable or even better performance than the PHYDYAS filter of $K = 4$.

4.2 The BER Test

The simulation parameters are set according to Table 4.1.6 of [14]. In simulations, two interference factors are taken into account.

(1) The carrier frequency offset (CFO) being set to 0.2 or a random number uniformly distributed in −0.2–0.2.
(2) In simulated CR-like scenarios, two users occupy half of the subchannels and posses power ratio 1:1 or 1:5. In the later case, the BER of the user with small power will be calculated.

Figures 2 and 3 show the BER simulations under different CFO effects and user power setup. In the case of power ratio 1:5, either 'CFO = 0.2' or random CFO will

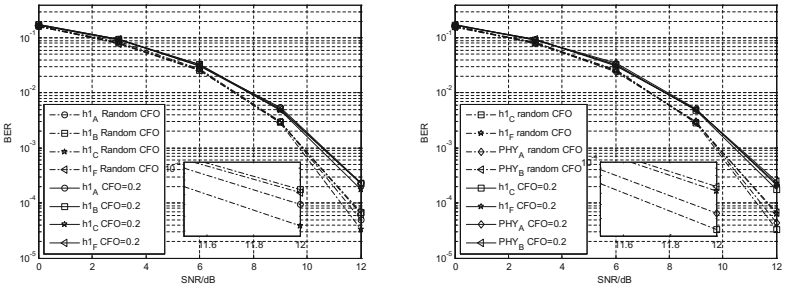

a. The proposed filters b. The proposed filters and the PHY filters

Fig. 2. The BER comparison for the filters in Tab.III: the case for power ratio 1:1.

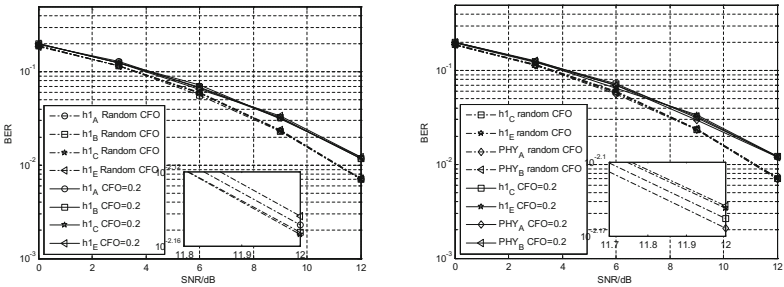

a. The proposed filters b. The proposed filters and the PHY filters

Fig. 3. The BER comparison for the filters in Tab.III: the case for power ratio 1:5.

cause severe interference and degrade the BER performance, yet the proposed filters show some superiority to the PHYDYAS filters. While in the case of power ratio 1:1, it is clear to see the BER difference between our prototype filter and the PHYDYAS filter. Moreover, we can find that the frequency selectivity is more important than the Nyquist condition, since the interferences caused by relaxed Nyquist condition are smaller than the residual interferences by CFO. As a conclusion, the $\mathbf{h}1_C$ is the best one and the $\mathbf{h}1_F$ provides a suitable tradeoff with reduced filter length.

5 Conclusions

Combining the NYQ filter optimization and the spectral factorization aimed at minimum stopband energy, this paper provides a flexible design for prototype filter in FBMC systems. From the examples and BER simulations, it is evident that the resulted nonlinear-phase SR Nyquist filter with relaxed Nyquist condition are superior to the widely-employed PHYDYAS filters. These filters have a flexible tradeoff for better frequency selectivity, a strengthened robustness against ICI, and the ability to reduce the filter length, which may benefit FBMC practical application in such as CR networks and burst transmission.

Acknowledgement. This paper was sponsored by the National NSF of China under grant No. 61471322.

References

1. Chávez-Santiago, R., Szydełko, M., Kliks, A., Foukalas, F.: 5G: the convergence of wireless communications. Wirel. Pers. Commun. **83**(3), 1617–1642 (2015)
2. Bellanger, M.: Physical layer for future broadband radio systems. In: 2010 IEEE Radio and Wireless Symposium (RWS), pp. 436–439 (2010)
3. Doré, J.B., Cassiau, N., Kténas, D.: Low complexity frequency domain carrier frequency offset compensation for multiuser FBMC receiver. In: 2014 European Conference on Networks and Communications (EuCNC), pp. 1–5 (2014)

4. Bellanger, M., Le Ruyet, D., Roviras, D., Terré, M., et al.: FBMC physical layer: a primer. PHYDYAS report. http://www.ict-phydyas.org/teamspace/internal-folder/special-session-at-crowncom-2010
5. Premnath, S.N., Wasden, D., Kasera, S.K., Patwari, N., et al.: Beyond OFDM: best-effort dynamic spectrum access using filterbank multicarrier. IEEE/ACM Trans. Netw. **21**(3), 869–882 (2013)
6. Schaich, F., Wild, T.: Waveform contenders for 5G - OFDM vs. FBMC vs. UFMC. In: 6th IEEE International Symposium on Communications, Control and Signal Processing (ISCCSP), pp. 457–460 (2014)
7. Sahin, A., Guvenc, I., Arslan, H.: A survey on multicarrier communications: prototype filters lattice structures implementation aspects. IEEE Commun. Surv. Tutor. **16**(3), 1312–1338 (2014)
8. Mirabbasi, S., Martin, K.: Overlapped complex-modulated transmultiplexer filters with simplified design and superior stopbands. IEEE Trans. Circuits Syst. II: Analog Digit. Signal Process. **50**(8), 456–469 (2003)
9. Farhang-Boroujeny, B.: A square-root Nyquist (M) filter design for digital communication systems. IEEE Trans. Signal Process. **56**(5), 2127–2132 (2008)
10. Davidson, T.: Enriching the art of FIR filter design via convex optimization. IEEE Signal Process. Mag. **27**(3), 89–101 (2010)
11. Lai, X., Lin, Z.: Optimal design of constrained FIR filters without phase response specifications. IEEE Trans. Signal Process. **62**(17), 4532–4546 (2014)
12. Hua, J., Wen, J., Lu, W., Li, F., et al.: Design and application of nearly Nyquist and SR-Nyquist FIR filter based on linear programming and spectrum factorization. In: 9th IEEE Conference on Industrial Electronics and Applications (ICIEA), pp. 64–67 (2014)
13. Viholainen, A., Ihalainen, T., Stitz, T.H., Renfors, M., Bellanger, M.: Prototype filter design for filter bank based multicarrier transmission. In: 17th European Signal Processing Conference, pp. 1359–1363 (2009)
14. Germany F.E.H., France A.C.: Final 5GNOW transceiver and frame structure concept D3.3. 5GNOW report. https://www.is-wireless.com/fp7-5gnow/